zek00315/zek4407d15z | xppws | S=1 | 1/24/15 | 9:01 | 4/C Fig: 3 | ArtID: 00238-14 | NLM: research-article | CE: jlo

Editor: Keeling | Section: Articles | Designation: T

EC Journals.ASM.org

The ADP/ATP Carrier and Its Relationship to Oxidative Phosphorylation in Ancestral Protist *Trypanosoma brucei*

AQ: au Anna Gnipová,[a,b] Karolína Šubrtová,[a,c] Brian Panicucci,[a] Anton Horváth,[b] Julius Lukeš,[a,c,d] Alena Zíková[a,c]

AQ: aff Biology Center, Institute of Parasitology, Czech Academy of Sciences, České Budějovice, Czech Republic[a]; Department of Biochemistry, Faculty of Natural Sciences, Comenius University, Bratislava, Slovakia[b]; Faculty of Science, University of South Bohemia, České Budějovice, Czech Republic[c]; Canadian Institute for Advanced Research, Toronto, Ontario, Canada[d]

The highly conserved ADP/ATP carrier (AAC) is a key energetic link between the mitochondrial (mt) and cytosolic compartments of all aerobic eukaryotic cells, as it exchanges the ATP generated inside the organelle for the cytosolic ADP. *Trypanosoma brucei*, a parasitic protist of medical and veterinary importance, possesses a single functional AAC protein (TbAAC) that is related to the human and yeast ADP/ATP carriers. However, unlike previous studies performed with these model organisms, this AQ: A **study showed that TbAAC is most likely not a stable component of either the respiratory supercomplex III+IV or the ATP synthasome but rather functions as a physically separate entity in this highly diverged eukaryote. Therefore, TbAAC RNA interference (RNAi) ablation in the insect stage of *T. brucei* does not impair the activity or arrangement of the respiratory chain complexes. Nevertheless, RNAi silencing of TbAAC caused a severe growth defect that coincides with a significant reduction of mt ATP synthesis by both substrate and oxidative phosphorylation. Furthermore, TbAAC downregulation resulted in a decreased level of cytosolic ATP, a higher mt membrane potential, an elevated amount of reactive oxygen species, and a reduced consumption of oxygen in the mitochondria. Interestingly, while TbAAC has previously been demonstrated to serve as the sole ADP/ATP carrier for ADP influx into the mitochondria, our data suggest that a second carrier for ATP influx may be present and active in the *T. brucei* mitochondrion. Overall, this study provides more insight into the delicate balance of the functional relationship between TbAAC and the oxidative phosphorylation (OXPHOS) pathway in an early diverged eukaryote.**

event

AQ: B The origination of an ADP/ATP carrier (AAC) was ~~a~~ crucial ~~event~~ in the evolution of the present-day mitochondrion that enabled it to become the powerhouse of the eukaryotic cell. Due to the activity of AAC, the energy-producing mitochondria can supply the cytosol with ATP molecules, which fuel most cellular reactions. AAC belongs to the well-defined family of mitochondrial (mt) carrier proteins that are located in the inner mt membrane and are involved in the transport of a wide range of metabolites (1). Under physiological aerobic conditions, AAC is responsible for the 1:1 counterexchange of mt ATP for cytosolic ADP (2).

mt ATP is produced mainly by the evolutionarily conserved biochemical pathway of oxidative phosphorylation (OXPHOS), which employs respiratory complexes I through IV to convert the redox energy of various mt substrates into an electrochemical proton gradient ($\Delta\psi m$) across the mt inner membrane. Respiratory complexes I (NADH-ubiquinone oxidoreductase) and II (succinate-ubiquinone oxidoreductase) are responsible for the oxidation of reduced NADH and $FADH_2$, respectively. The electrons derived from these biochemical processes continue along the electron transport chain as they are sequentially passed to coenzyme Q, complex III (ubiquinol-cytochrome *c* oxidoreductase), cytochrome *c*, complex IV (cytochrome *c*-O_2 oxidoreductase), and finally oxygen, the terminal electron acceptor. The electron movement up the redox potential is coupled with proton translocation into the intermembrane space, resulting in the $\Delta\psi m$. The protons are then permitted to flow down their concentration gradient and return to the mt matrix via F_oF_1-ATP synthase, which harnesses this potential energy to rotate its macromolecular enzymatic machine to generate ATP from ADP and inorganic phosphate (P_i). These two substrates are transported into the mt matrix via their carrier proteins, AAC and the phosphate carrier (P_iC).

In some eukaryotes, OXPHOS complexes form higher-order assemblies or supercomplexes to promote faster diffusion of the substrate molecules and increase respiration efficiency (3). Complexes I, III, and IV have been found to form different types of supercomplexes (i.e., I+III_2, III_2+IV_2, and I+III_2+IV_{1-4}) in a wide range of organisms (4). Moreover, F_oF_1-ATP synthase forms dimers that appear to be crucial for mt inner membrane folding and consequently crista morphology (5, 6). Though the translocase activity of AAC is self-contained within a single protein (7), in yeast, this transporter can be found also as a homodimer (8) or as a component of supercomplexes composed of complexes III and IV and the TIM23 translocase (9, 10). Moreover, in rat mitochondria, a minor population of AAC was also detected in a supercomplex comprised of the F_oF_1-ATP synthase and P_iC, forming the ATP synthasome (11, 12).

Organization of proton translocation OXPHOS components into supercomplexes seems to be absent in the early-branching protist *Trypanosoma brucei*, a member of the eukaryotic supergroup Excavata (13). *T. brucei* is a flagellated parasite of major medical and veterinary importance, causing sleeping sickness in

Received 22 October 2104 **Accepted** 16 January 2015

Accepted manuscript posted online ●●●

Citation Gnipová A, Šubrtová K, Panicucci B, Horváth A, Lukeš J, Zíková A. 2015. The ADP/ATP carrier and its relationship to oxidative phosphorylation in ancestral protist *Trypanosoma brucei*. Eukaryot Cell 14:000–000. doi:10.1128/EC.00238-14.

Address correspondence to Alena Zíková, azikova@paru.cas.cz.

Supplemental material for this article may be found at http://dx.doi.org/10.1128/EC.00238-14.

doi:10.1128/EC.00238-14

humans and nagana in cattle (14, 15). The morphology and biochemical activity of its single mitochondrion differs dramatically between life stages as the parasite alternates between the insect vector and a mammalian host (16). Since amino acids (e.g., proline and threonine) in the midgut of the insect vector constitute the main energy source available to the procyclic form of trypanosomes (PF), they maintain a well-developed mitochondrion with abundant cristae, Krebs cycle enzymes, and a fully active cytochrome-mediated respiratory chain that is coupled to ATP production by F_oF_1-ATP synthase (17, 18). In addition to OXPHOS, significant amounts of ATP are also produced by mt substrate phosphorylation (19). In this life stage, TbAAC works in its forward mode, importing ADP into the organelle while concurrently exporting ATP to the cytosol.

In contrast, the mammalian bloodstream stage (BS) relies solely on the host's abundant glucose, which is catabolized by the inefficient glycolysis pathway to meet its energy demands (20). The conventional respiratory pathway is absent, and the mt reducing equivalents are reoxidized by another route composed of an alternative oxidase and alternative dehydrogenase (21, 22). Importantly, this process is not coupled to proton translocation; thus, the $\Delta\psi m$ is maintained by the reverse activity of F_oF_1-ATPase, while AAC presumably supplies the enzyme with the requisite ATP substrate (23, 24).

The *T. brucei* genome encodes two different proteins, Tb927.8.1310 and TbAAC, with the latter being represented by three identical and consecutively arranged genes (Tb927.10.14820, -30, and -40) and showing significant amino acid sequence similarity to functionally characterized AACs from other eukaryotes (25). Importantly, TbAAC exhibits biochemical properties and ADP/ATP exchange kinetics similar to the main yeast carrier, AAC2, while Tb927.8.1310 lacks the canonical sequence features required for ADP/ATP exchange activity (26). Furthermore, RNA interference (RNAi) studies demonstrated that TbAAC is essential for the growth of PF cells and therefore must function as the main ADP/ATP carrier in PF mitochondria (26).

Since PF *T. brucei* represents an ancestral eukaryote possessing typical mt functions (27), we explored the relationship between TbAAC and the other OXPHOS components. Our analysis of the structural and functional interactome of TbAAC reveals that it exists as a physically separate entity that could not be detected as a stable component of either respiratory complex III or IV or F_oF_1-ATP synthase. Furthermore, the activities of the OXPHOS complexes were not impaired upon TbAAC RNAi silencing. However, TbAAC depletion induced a cellular ADP/ATP imbalance followed by low levels of cytosolic ATP, higher $\Delta\psi m$, elevated quantities of reactive oxygen species (ROS), and reduced mt oxygen consumption. In summary, the apparent lack of a tight physical interaction between TbAAC and the OXPHOS pathway hints at the unique functional relationships between these fundamental components of the PF *T. brucei* mt bioenergetics.

MATERIALS AND METHODS

Plasmid construction. To create the TbAAC (Tb927.10.14820, Tb927.10.14830, and Tb927.10.14840) RNAi construct, a 901-bp fragment that is identical for each of the TbAAC genes was PCR amplified from *T. brucei* strain 427 genomic DNA with the oligonucleotides CTC GAG CGG ATA AAA AGC GG (FW) and GGA TCC TCC ACA TAA ATG GGT (REV), utilizing the respective XhoI and BamHI restriction sites inherent in the primers (underlined). The digested amplicon was then cloned into the p2T7-177 plasmid (28). For the inducible expression of TbAAC fused with a C-terminal v5 tag, the TbAAC coding sequence was PCR amplified with the primers CAC AAG CTT ATG ACG GAT AAA AAG and CAC GGA TCC ATT CGA TCT GCG CCA C and then cloned into the pT7_v5 (29) vector using the HindIII and BamHI restriction sites (underlined). The construction of the pLEW79MHTAP vectors for the tetracycline (Tet)-inducible expression of tandem affinity purification (TAP)-tagged F_oF_1-ATPase subunits p18 (Tb927.5.1710) and β (Tb927.3.1380) was described previously (18). For the constitutive expression of firefly luciferase in the cytosol of PF *T. brucei*, the luciferase reporter gene was PCR amplified from pLEW79 vector using the primers GC AAG CTT ATG GAA GAC GCC AAA AAC (FW) and GCT GGA TCC TTA CTT CTT GGC CTT TAT G (RV). The PCR amplicon was subcloned to PGEM-T Easy vector (Promega) and cloned into pHD1344tub plasmid (a kind gift from Achim Schnaufer) using HindIII and BamHI restriction sites. AQ: C AQ: D

Cell growth, transfection, and RNAi induction. PF *T. brucei* strain 29-13 cells are transgenic for both the T7 RNA polymerase and the Tet repressor (30). Grown *in vitro* at 27°C in SDM-79 medium containing hemin (7.5 mg/ml), hygromycin (25 μg/ml), G-418 (10 μg/ml), and 10% fetal bovine serum, these cells were used as the parental cell line for p2T7-177 and pT7_v5 transfections. Both of these plasmids were linearized with NotI and stably transfected into the minichromosome 177-bp repeat region and the rDNA spacer, respectively (28, 31). Cell lines containing p2T7-177 were selected with phleomycin (2.5 μg/ml), while cells transfected with the pT7_v5 plasmid were selected with puromycin (1 μg/ml). The TbAAC RNAi cell line was used as a parental cell line for pHD1344tub transfection and selected with puromycin. The inducible expression of double-stranded RNA (dsRNA) or the TbAAC_v5-tagged protein was triggered by the addition of 1 μg/ml Tet to the medium. Growth curves were generated by measuring the cell density of Tet-treated and untreated cultures using the Z2 cell counter (Beckman Coulter Inc.). Throughout the experiments, cells were split daily to ensure that they continuously maintained an exponential growth phase of 10^6 to 10^7 cells/ml.

Immunoprecipitation and affinity purification methods. Mitochondria from TbAAC_v5, β_TAP, and p18_TAP cell lines were hypotonically purified from 4×10^9 noninduced and Tet-induced cells (day 2) as described earlier (32). mt pellets were resuspended in the appropriate buffer (TbAAC_v5 mitochondria in IPP100 buffer consisting of 100 mM KCl, 10 mM $MgCl_2$, and 10 mM Tris-HCl, pH 7.2; TAP mt pellets in another IPP100 buffer comprised of 100 mM KCl, 0.1% NP-40 and 10 mM Tris-HCl, pH 8.0), which was also supplemented with Complete protease inhibitors (Roche). Next, the samples were lysed with digitonin (at a detergent/protein ratio of 1 mg/mg) for 1 h on ice and then spun down (15,000 × *g*, 1 h, 4°C). The TbAAC_v5-tagged complexes were purified using magnetic beads (Dynabeads M-280, sheep anti-mouse IgG) charged with monoclonal anti-v5 antibody. The mt lysate was incubated with the charged beads for 2 h (4°C). The beads were washed three times in PBS-T (phosphate-buffered saline with 0.05% Tween 20) and twice with IP100 buffer before the bound protein complexes were released by the addition of SDS-PAGE loading buffer and boiling (97°C, 10 min). The β_TAP and p18_TAP cleared lysates were incubated for 2 h with IgG Sepharose 6 Fast Flow beads (GE Healthcare), which bind to protein A, a part of the TAP tag. The beads were then washed three times with IPP100 and once with a TEVCB buffer (100 mM KCl, 0.1% NP-40, 0.5 mM EDTA, 1 mM dithiothreitol [DTT], 10 mM Tris-HCl [pH 8.0]). The bound protein complexes were released by AcTEV protease (Invitrogen) cleavage (3 h, 16°C). All eluates were fractionated by SDS-PAGE and analyzed by Western blotting.

Glycerol gradient sedimentation. As described in an earlier publication (33), mt vesicles from 1×10^9 cells were isolated by hypotonic cell lysis and then incubated in a glycerol gradient lysis buffer (10 mM Tris-HCl [pH 7.2], 10 mM $MgCl_2$, 200 mM KCl, 1 mM DTT) containing dodecyl maltoside at a ratio of 1 mg detergent to 1 mg protein. The lysates were cleared by centrifugation (twice at 16,000 × *g* for 30 min at 4°C), loaded onto an 11-ml 10-to-30% glycerol gradient, and sedimented by ultracentrifugation (SW40 rotor; Beckman Instruments) at 38,000 × *g* for 12 h. Fractions (500 μl) were collected and stored at −70°C.

luciferase (LUC) expressing

Electrophoresis and Western blot analysis. Two-dimensional (2-D) PAGE analysis was performed by fractionating 100 μg of mt lysate on a 3 to 8% high-resolution clear native (hrCN) PAGE gel, which was then further resolved on a 10% Tricine–SDS-PAGE gel (34). After electrophoresis, the proteins were transferred onto a nitrocellulose membrane and probed with specific antibodies.

Protein samples from whole-cell lysates, mt lysates, and glycerol gradient fractions were separated on SDS-PAGE gels, blotted onto nitrocellulose membrane, and probed with the appropriate monoclonal (MAb) or polyclonal (PAb) antibody. This was followed by incubation with a secondary horseradish peroxidase (HRP)-conjugated anti-rabbit or anti-mouse antibody (1:2,000; Bio-Rad). Proteins were visualized using the Clarity Western enhanced chemiluminescence (ECL) substrate (Bio-Rad) on a ChemiDoc instrument (Bio-Rad). When needed, membranes were stripped at 50°C for 30 min in a stripping buffer (62.5 mM Tris-HCl [pH 6.8], 100 mM mercaptoethanol, 2% SDS) and reprobed. The PageRuler prestained protein standard (Fermentas) was used to determine the sizes of detected bands. The following primary antibodies were used in this study: a MAb against the paramyxovirus v5 tag (Invitrogen) (1:1,000), a PAb against the human c-*myc* protein (Sigma) (1:1000), a MAb against the North American firefly luciferase (Invitrogen) (1:1,000), and a PAb against the *Leishmania tarentolae* cytochrome *c* oxidase subunit IV (trCOIV) (1:1,000) (35). Furthermore, specific antibodies raised against *T. brucei* antigens were utilized: anti-enolase PAb (1:1,000) (36), anti-mt Hsp70 MAb (1:2,000) (37), anti-apocytochrome *c* PAb (1:1,000) (38), anti-COVI PAb (1:1,000) (33), anti-ATPaseTb2 PAb (1:1,000) (39), anti-β PAb (1:2,000), and p18 PAb (1:1,000). Additional *T. brucei* antibodies against TbVDAC (1:1000), putative TbP_iC (Tb927.9.10310; 1:1,000) (25), TbAAC (1:1,000), and complex III subunit Rieske (1:1,000) were prepared commercially (Davids Biotechnology) by administering antigen-specific oligopeptides (TbVDAC, VDK SLK PGV LIT HS; TbP_iC, SHP ADM LVS ARG KAS NVG KS; TbAAC, VDA LKP IYV EWR RSN; and complex III subunit Rieske, LSA LKH PET DEA RFP DHR E) to rabbits following a standard immunization protocol.

***In vitro* and in-gel activity measurements of respiratory complexes.** mt vesicles isolated from 5×10^8 trypanosomes were lysed with 2% dodecyl maltoside, and the cytochrome *c* oxidase activity was determined *in vitro* by measuring the change in absorbance of cytochrome *c* as it became oxidized after passing its electrons to cytochrome *c* oxidase (40). Cytochrome *c* reductase activity was determined in a similar way; this time, the reduction of cytochrome *c* was measured when reduced decylubiquinone (Sigma) was added as an electron donor and cytochrome *c* reductase transferred those electrons to cytochrome *c* (33). In parallel, the same dodecyl maltoside lysed mitochondrion samples were resolved (100 μg of protein per lane) on either a 6% blue native (BN) PAGE gel or a 2 to 12% BN PAGE gel to detect cytochrome *c* oxidase and F_oF_1-ATPase activities by following in-gel assays, as described in earlier work (41). The ATPase activity was measured in digitonin-extracted mitochondria as described elsewhere (18).

ATP production and ATPase assays. ATP production in digitonin-extracted mitochondria was measured following a protocol described previously (42). Briefly, crude mt fractions from the RNAi knockdown cell lines were obtained by digitonin extraction (43). ATP production in these samples was induced by the addition of 67 μM ADP and a 5 mM concentration of one of the following substrates: succinate, pyruvate, or α-ketoglutarate. The mt preparations were preincubated for 10 min on ice with the inhibitors malonate (6.7 mM) and atractyloside (33 μg/ml). The concentration of ATP was determined by a luminometer (Orion II; Berthold Detection Systems) using the CLS I ATP bioluminescence assay kit (Roche Applied Science). ATPase activity was measured with the Sumner assay (44), which is based on the release of free phosphate when ATP is hydrolyzed by the enzyme, as defined earlier (24).

AQ: E

In vivo ATP measurement. Cytosolic ATP was measured *in vivo* using ATP-dependent luciferase bioluminescence. The method was adapted for *T. brucei* cells from published protocols (45, 46). Briefly, equal numbers of PF LUC-TbAAC noninduced and RNAi-induced cells (5×10^6) were harvested (1,300 × *g*, 10 min, room temperature), washed with PBS (pH 7.4), and resuspended in PBS-LUC buffer (PBS, 1 mM $CaCl_2$, 20 mM $MgCl_2$ ~~[pH 7.7]~~). The emission of light was triggered by addition of D-luciferin (50 μM; Sigma) and immediately measured on a microplate luminometer. The cells exhibited a maximum luminescence signal 1 min after D-luciferin addition. Then the signal remained stable for at least 20 min afterwards, and it decayed at very low rate.

AQ:F-G

***In vivo* analysis of oxygen consumption, mt membrane potential, and ROS.** Oxygen consumption of logarithmically growing cells was determined with a Clark-type polarographic electrode (1302 microcathode oxygen electrode, model 782; Strathkelvin Instruments) as described previously (41). Tetramethylrhodamine ethyl ester (TMRE; 60 nM; Molecular Probes) uptake was used to measure the mt membrane potential, whereas 2′,7′-dichlorofluorescin diacetate (DCFH-DA; 10 μM; Sigma) was implemented to monitor ROS production. Both methods were performed as described earlier (41).

Nuclear and kinetoplast DNA staining. Logarithmically grown noninduced and RNAi-induced cells were pelleted by centrifugation, washed, fixed with 4% formaldehyde, and treated with DAPI (4′,6-diamidino-2-phenylindole; Sigma) to visualize nuclear and mt DNA. The images of the stained cells and their fluorescence were captured on a Axioplan2 imaging fluorescence microscope (Zeiss) equipped with a charge-coupled device (CCD) camera and the appropriate filters.

RESULTS

2-D PAGE reveals that a minor proportion of TbAAC migrates at higher molecular weights. To investigate potential TbAAC interactions within the mt inner membrane, purified mt vesicles were solubilized using digitonin and dodecyl maltoside at different detergent/protein ratios and then resolved by 2-D electrophoresis. These detergents are mild, nonionic surfactants that are capable of releasing membrane embedded protein complexes without disrupting internal protein-protein interactions. Furthermore, these surfactants are commonly applied in 2-D PAGE analyses and were extensively used to determine the AAC interactome in mammalian and yeast cells (9, 47–49). Therefore, detergent-solubilized mt complexes were resolved in a two-step process: by high-resolution clear native (hrCN) PAGE in the first dimension, followed by a second dimension of denaturing Tricine–SDS-PAGE. After proteins had been transferred to a nitrocellulose membrane, the Western blot was probed with an anti-TbAAC antibody (Fig. 1A). Interestingly, while a significant majority of TbAAC was detected in the lower-molecular-weight region, which likely depicts the monomeric protein, a portion of the signal also extended into a range of much higher molecular masses, culminating in two distinct peaks (Fig. 1A, middle, arrowheads). This signal is most intense when digitonin is used at a ratio of 1 mg/1 mg mt proteins, although comparable results were obtained when the isolated mitochondria were solubilized with dodecyl maltoside (data not shown).

F1

While it is possible that these large TbAAC complexes are just aggregates of AAC that have not been separated with these mild detergents, we aimed to address whether these higher-molecular-weight TbAAC complexes might colocalize with any of the previously identified OXPHOS components, specifically with the respiratory complex IV and/or the F_oF_1-ATP synthasome (complex V and P_iC). A Western blot containing mt proteins resolved by the same 2-D PAGE conditions (1 mg digitonin/1 mg mt proteins) was immunodecorated with specific antibodies that recognize subunit COVI of complex IV, subunit β of complex V, and TbP_iC to identify the complexes listed above, respectively (Fig. 1B). No-

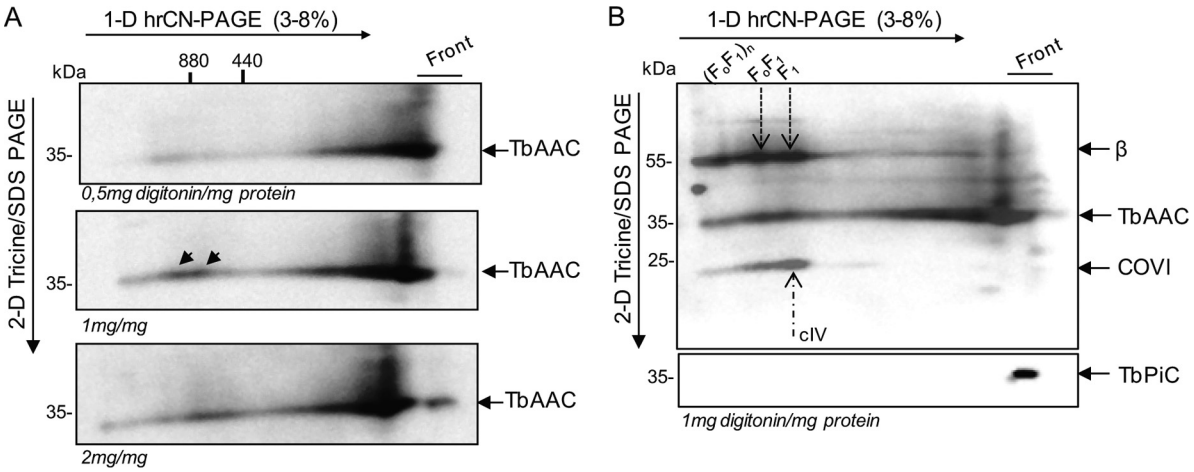

FIG 1 TbAAC colocalizes with higher-molecular-weight complexes. (A) The hypotonically purified mitochondria were solubilized using digitonin (0.5 mg, 1 mg, and 2 mg detergent/mg protein) and separated on a 3 to 8% hrCN PAGE. Isolated lanes from these native gels were further processed in the second dimension by denaturing Tricine–SDS-PAGE, and the gel was blotted on a nitrocellulose membrane for immunodetection using a polyclonal anti-TbAAC antibody. "Front" indicates the leading edge of the first-dimensional gel. The sizes of the native molecular mass markers are indicated on top of the first panel. The protein marker for the second dimension is indicated on the left. (B) The nitrocellulose membrane containing mitochondria lysed with 1 mg digitonin/mg mt protein was stripped and further probed individually with trypanosome-specific polyclonal antibodies against subunit COVI (complex IV), subunit β (F_oF_1-ATP synthase), and P_iC. The positions of monomeric and oligomeric F_oF_1-ATP synthase and complex IV are denoted by arrows. The resulting compilation of Western images was overlaid using Adobe Photoshop.

tably, the peak signals detected for complex IV and F_oF_1-ATP synthase (Fig. 1B, dashed arrows) approximately colocalize with the higher-molecular-weight TbAAC bands, offering indirect proof that a minor fraction of TbAAC may interact with these protein complexes. Upon closer inspection, the main peak of complex IV and F_1 seems to lead the AAC peaks. While the trailing edge of the smear for cytochrome *c* oxidase does overlap the largest AAC peak, this portion of AAC better aligns with the distinct peak of F_oF_1-ATP synthase. However, TbP_iC, a key component of the ATP synthasome, is clearly confined to the dye front of the hrCN PAGE. This observation weakens the possibility of the existence of a canonical ATP synthasome composed of complex V, AAC, and P_iC in trypanosomes.

TbAAC is not a stable component of respiratory complex III, IV, or V. While the observed colocalization of TbAAC with cytochrome *c* oxidase and F_oF_1-ATP synthase in 2-D hrCN–Tricine–SDS-PAGE is intriguing, we wanted to further verify a direct and stable interaction between these components via immunoprecipitation experiments. Therefore, the ectopic expression of a C-terminally v5-tagged TbAAC protein was induced by Tet in the PF 29-13 cell line. The tagged TbAAC_v5 was immunoprecipitated using magnetic beads charged with anti-mouse IgG and a specific anti-v5 monoclonal antibody. Bound TbAAC_v5 proteins were then eluted from the beads by SDS treatment, and the specificity of the reaction was confirmed by TbAAC Western blot analysis of immunoprecipitated material from noninduced and Tet-induced cells. While no TbAAC signal was detected in the eluate from noninduced cells, a band of the expected size was visible in the sample from Tet-induced *T. brucei* cells (Fig. 2A). Therefore, the obtained eluates were further examined using specific antibodies to detect core subunits of complex III (Rieske), IV (trCOIV), and F_oF_1-ATP synthase (β). No signal for Rieske or trCOIV was detected, indicating that there is no stable interaction between TbAAC and complex III or IV (Fig. 2A) under these conditions. The initial analysis concerning a possible interaction with the F_oF_1-ATP synthase was quite optimistic, as subunit β was enriched in the eluate from Tet-induced TbAAC_v5 cells, even though a basal level was also detected in the noninduced sample. Therefore, to determine if subunit β is just a spurious contaminant, we employed cell lines wherein either subunit β or p18 is TAP tagged to perform a reciprocal analysis involving the affinity purification of F_oF_1-ATP synthase, as previously described (18) (Fig. 2B). Western blot analysis using specific antibodies against either the tag (anti-c-*myc*) or F_oF_1-ATP synthase (F_1 moiety, subunit β and p18; F_o moiety, ATPaseTb2) (39) validated a successful purification, while a specific antibody against TbAAC was implemented to detect if there is an interaction between this protein and F_oF_1-ATP synthase. The absence of TbAAC in the eluates demonstrates that this protein does not stably associate with F_oF_1-ATP synthase (Fig. 2B) when it is purified in this manner.

TbAAC is essential for the growth of PF *T. brucei* cells. Since we were not able to detect any stable structural interactions for TbAAC with *T. brucei* respiratory complexes IV and V, we next explored the possibility of functional associations between this protein and the same OXPHOS complexes. Therefore, we created a TbAAC RNAi cell line in PF 29-13 *T. brucei* cells that is capable of inducible dsRNA expression when triggered by the addition of Tet to the culture medium. A significant growth phenotype was detected in the TbAAC-depleted cells by the fourth day of RNAi induction (Fig. 3A). This result emphasizes the importance of TbAAC as the major ADP/ATP carrier in *T. brucei* mitochondria and its irreplaceable function in the PF stage of the parasite. The efficiency of the RNAi was verified by Northern blotting using a transcript-specific probe, demonstrating that the TbAAC mRNA was significantly reduced after only 2 days of RNAi induction (Fig. 3A, inset). The targeted knockdown of TbAAC was further confirmed by Western blotting of whole-cell lysates harvested from noninduced and RNAi-induced cells (Fig. 3B, top). Equivalent cell numbers were loaded for each sample, and then cells were analyzed with an anti-mt Hsp70 monoclonal antibody to normal-

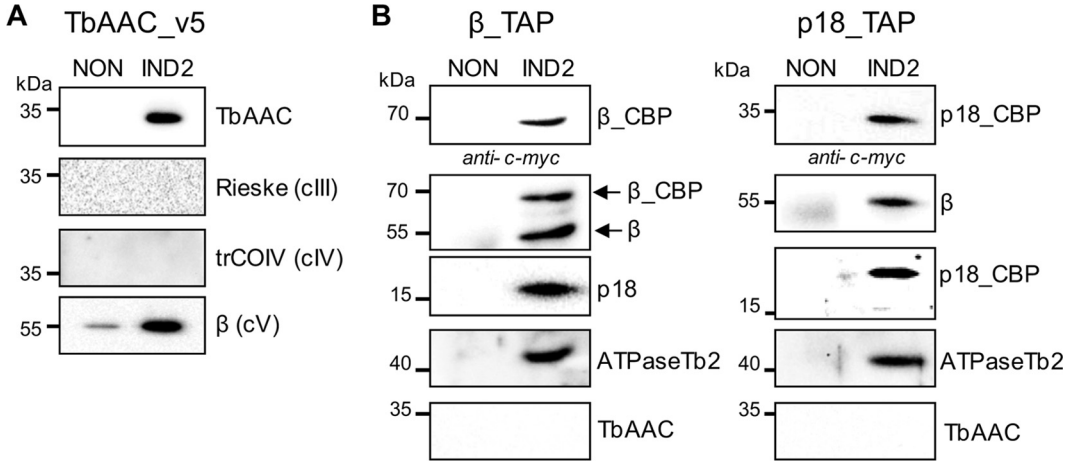

FIG 2 TbAAC does not copurify with complex IV or F_oF_1-ATP synthase. (A) TbAAC_v5-tagged complexes were purified using magnetic beads (Dynabeads M-280, sheep anti-mouse IgG) charged with a monoclonal anti-v5 antibody. The tagged protein complexes were purified from noninduced (NON) cells and 2-day Tet-induced cells (IND2) containing the regulatable ectopic v5-tagged TbAAC protein. The tagged protein complexes were eluted with SDS-PAGE loading buffer, fractionated by SDS-PAGE, and examined by Western blotting. The presence of the tagged TbAAC_v5 was verified using an anti-TbAAC antibody (top). The association of TbAAC_v5 with core subunits of complex III (Rieske), IV (trCOIV), and F_oF_1-ATPase (β) was determined using specific antibodies. The applicable sizes of the protein marker are indicated on the left. (B) F_oF_1-ATP synthase complexes were purified using tandem affinity purification from noninduced (NON) cells and cells induced for 2 days (IND2) to express the ectopically tagged subunits β_TAP (left) and p18_TAP (right). Tagged F_oF_1-ATP synthase complexes were purified by IgG affinity chromatography, eluted by TEV protease, resolved by SDS-PAGE, and examined by Western blotting. The presence of cleaved bait proteins now containing just the calmodulin-binding protein (CBP) and c-*myc* epitope tag, β_CBP and p18_CBP, was verified by an anti-c-*myc* antibody. Blots probed with antibodies specific to subunits β, p18, and ATPaseTb2 demonstrate that the TEV eluates contain components of both the F_1 and F_o moieties of the F_oF_1-ATP synthase (endogenous and TAP tagged), while Western blots immunodecorated with an anti-TbAAC antibody demonstrate that the ADP/ATP transporter is not detectable in β- and p18-tagged complexes. Noninduced cells were used as a negative control for any nonspecific protein binding during the IgG affinity purification. The relevant sizes of the protein marker are indicated on the left.

ize for equal loading. Finally, after being probed with an antibody against TbAAC, the Western blot exhibited reductions of the targeted protein by 40% and 71% at days 2 and 3 of RNAi induction, respectively (Fig. 3B, top).

Knockdown of TbAAC does not impair the steady state, structural integrity, and enzymatic activities of OXPHOS complexes. With the established TbAAC RNAi cell line, we examined if the steady-state abundance of specific core subunits of the OXPHOS complexes are affected upon efficient TbAAC depletion. Trypanosomatid-specific antibodies raised against subunits of complexes III (apoC and Rieske), IV (trCOIV and COVI), F_oF_1-ATP synthase (β), and TbP_iC were utilized to monitor the stability of these components over time in whole-cell lysates (Fig. 3B). No major changes were observed for any of the examined proteins except for TbP_iC, which was detected as a double band running around 35 kDa (Fig. 3B, bottom). Since the lower band disappeared and an interaction between the AAC and P_iC proteins was reported in the mammalian system (11), it was important to elucidate which band is specific for TbP_iC. Therefore, we created a TbP_iC RNAi cell line, in which the upper band is abated during dsRNA induction, demonstrating that TbP_iC (predicted mass, 34.3 kDa) migrates just above the 35-kDa protein marker (see Fig. S1A in the supplemental material) and thus is not affected by the knockdown of TbAAC (Fig. 3B, bottom). Hence, the TbP_iC antibody cross-reacts with TbAAC, resulting in a doublet where the upper band is TbP_iC and the lower band is TbAAC (see Fig. S1B in the supplemental material). This cross-reactivity was quite unexpected because the best match from a ClustalW alignment of the TbP_iC peptide antigen with TbAAC (see Fig. S1C in the supplemental material) shares less than 22% identity.

AQ: H

While the steady-state abundance of a few individual subunits of complexes III, IV, and F_oF_1-ATP synthase was unchanged upon the depletion of TbAAC, we wanted to verify that the integrity of these complexes was maintained by analyzing their sedimentation profiles on glycerol gradients. Mitochondria isolated from noninduced cells and RNAi cells induced for 5 days (IND5) were lysed by dodecyl maltoside (2 mg detergent/mg mt protein) and fractionated on a 10-to-30% glycerol gradient (Fig. 3C). The resolved fractions were then analyzed by Western blotting, utilizing the anti-TbAAC antibody to confirm a successful knockdown and the anti-apoC, anti-trCOIV, anti-subunit β, and anti-TbP_iC antibodies to illustrate the sedimentation profile for complexes III and IV, F_oF_1-ATP synthase, and the phosphate carrier. Notably, the sedimentation profiles of the examined complexes and TbP_iC were unaltered between the noninduced and RNAi-induced samples (Fig. 3C). Thus, silencing of TbAAC does not interfere with the assembly and/or stability of the examined OXPHOS complexes.

The evolutionary benefit of the interaction between AAC and various components of OXPHOS is that it increases the efficiency of these machines. Indeed, when AAC was depleted in yeast cells, it was shown to affect the activity of complexes III and IV, which were decreased by 15% and 55%, respectively (9). Therefore, specific *in vitro* enzymatic activity assays were performed with mt extracts obtained from noninduced and TbAAC RNAi-induced cells and revealed no significant differences in the activities of respiratory complexes III and F_oF_1-ATP synthase, while the activity of complex IV was slightly increased (i.e., cytochrome *c* reductase activity was 107% ± 11%, cytochrome *c* oxidase activity was 126% ± 11%, and ATP hydrolase activity was 118% ± 5% in RNAi-induced cells relative to activities in noninduced cells). Furthermore, the enzymatic activities of complexes IV and V were also examined using native 1-D BN PAGE followed by in-gel ac-

AQ: I

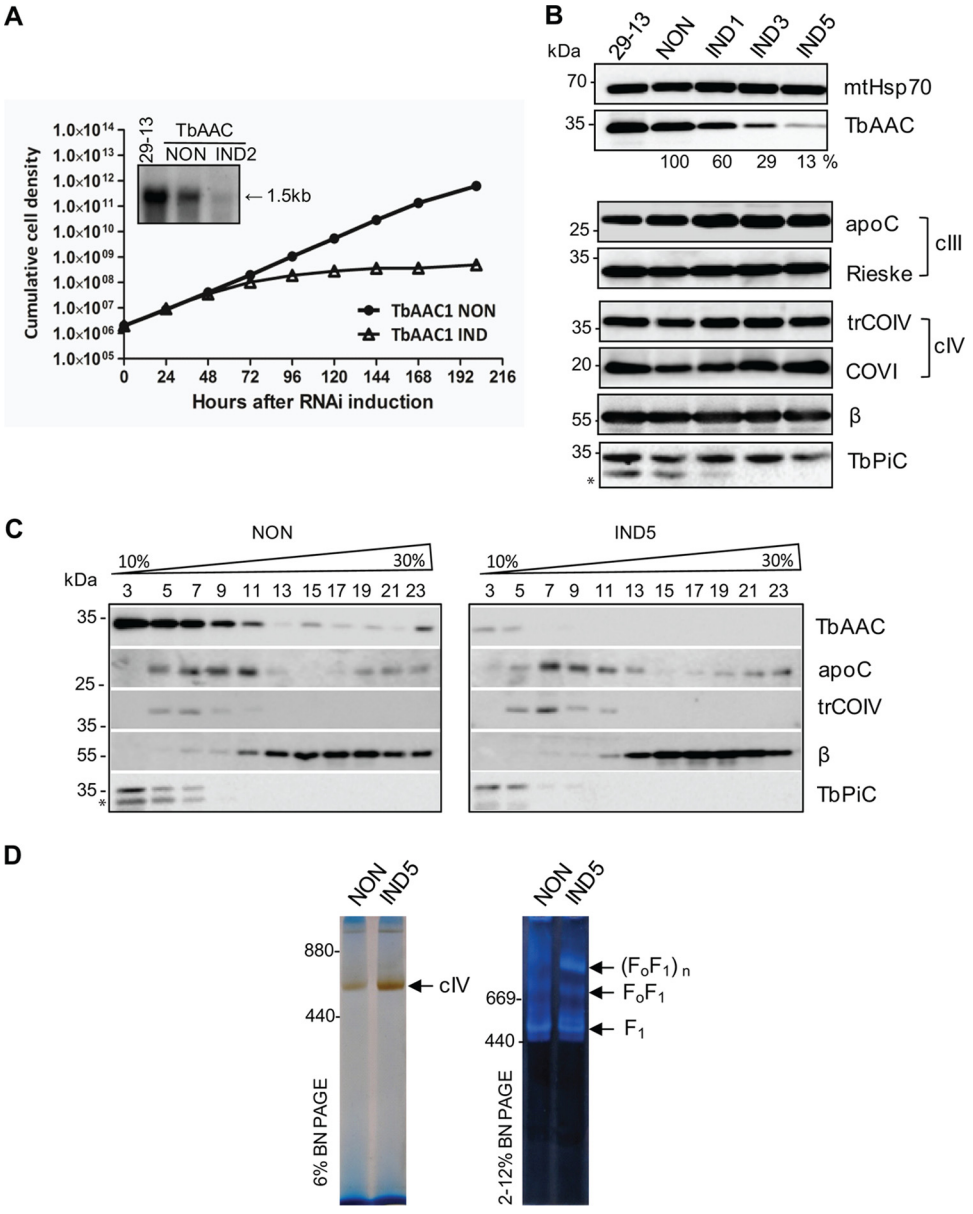

COLOR

FIG 3 TbAAC is essential for *in vitro* growth but does not impair either the steady-state abundance or sedimentation profile of OXPHOS complexes or the in-gel activities of complex IV and F_oF_1-ATPase. (A) Growth curves of the noninduced (NON) and Tet-induced (IND) TbAAC RNAi procyclic *T. brucei* cell lines. Cells were maintained in the exponential growth phase (between 10^6 and 10^7 cells/ml), and cumulative cell numbers were calculated from daily counts that incorporated each subsequent dilution factor. The inset depicts a Northern blot analysis of TbAAC mRNA levels in the parental 29-13 cells, noninduced cells (NON), and cells induced for 2 days of RNAi (IND2). (B) The steady-state abundance of TbAAC, core subunits of complex III (apoC and Rieske), complex IV (trCOIV and COVI), F_oF_1-ATP synthase (β), and TbP_iC in noninduced (NON) TbAAC RNAi cells and those induced for 1, 3, and 5 days (IND1, IND3, and IND5) was determined by Western blotting using specific polyclonal antibodies. The numbers beneath the TbAAC blot represent the abundance of immunodetected TbAAC, expressed as a percentage of the noninduced samples after normalization to the loading control, mt Hsp70. The relevant sizes of the protein marker are on the left. The TbP_iC antiserum cross-reacts with TbAAC, and this band is indicated with an asterisk. (C) The sedimentation profiles of TbAAC, TbP_iC, complexes III and IV, and F_oF_1-ATP synthase were examined using Western blot analysis of glycerol gradient fractions. Mitochondria from non-RNAi-induced cells (NON) and cells induced for 5 days (IND5) were lysed with dodecyl maltoside. An equal amount of the cleared lysate from 1×10^9 trypanosomes was loaded on each 10-to-30% glycerol gradient. Western analyses with trypanosomatid-specific antibodies raised against AAC, P_iC, apoC (complex III), trCOIV (complex IV), and subunit β (F_oF_1-ATP synthase) depict the sedimentation profile of the examined OXPHOS complexes. The glycerol gradient fractions are numbered, and the sizes of the protein marker are indicated. An asterisk designates the TbAAC band that cross-reacts with the TbP_iC antiserum. (D) In-gel complex IV and F_oF_1-ATP synthase activity staining after TbAAC repression. mt preparations from noninduced (NON) and RNAi cells Tet-induced for 5 days (IND5) were solubilized using dodecyl maltoside and separated either by 6% BN PAGE for complex IV staining or by 3-to-12% BN PAGE for F_oF_1-ATPase staining. The arrows denote bands visualized by the specific activity staining. The sizes of high-molecular-weight markers (ferritin and its dimer; Sigma) are on the left (in ~~thousands~~).

AQ: P

tivity staining (Fig. 3C). Complex IV was visualized as a single band at ~700 kDa (13, 41), while F_oF_1-ATP synthase was depicted by both the free F_1 moiety and multimeric F_oF_1 complexes (18). Though a slight increase of complex IV activity was detected, no major changes in the size and activity of the F_oF_1-ATP synthase were revealed when TbAAC was abated (Fig. 3C).

In summary, an efficient knockdown of TbAAC did not trigger any visible changes in the steady-state abundance of TbP_iC and selected subunits of OXPHOS complexes. Furthermore, no major differences were found in the sedimentation profiles, and no reductions in *in vitro* enzymatic activities of the examined complexes were detected. Thus, it seems that TbAAC exists as a physically separate entity in the inner mt membrane with no effect on the structural arrangement of OXPHOS components.

TbAAC is responsible for the import of ATP and ADP into the mitochondrion. Under aerobic conditions, the most important role of the ADP/ATP carrier is to sustain the cellular ATP homeostasis by enabling the 1-to-1 exchange of cytosolic ADP for mt ATP produced by an active OXPHOS pathway. However, when the cell finds itself under anaerobic or microaerobic conditions, the OXPHOS activity is usually downregulated and the ADP/ATP carrier works in reverse, resulting in a 1:1 exchange of mt ADP for cytosolic ATP (50).

To test if TbAAC is fully or only partially responsible for the influx of ADP into the organelle, an mt ATP production assay was performed. The isolated mitochondria from noninduced and RNAi-induced cells were incubated with ADP, free phosphate, and a suitable respiratory substrate, such as succinate, to trigger oxidative phosphorylation, or either α-ketoglutarate or pyruvate/succinate, to trigger one of two specific substrate phosphorylation reactions. Upon the addition of all these substrates, the mitochondria are energized and produce ATP, which can be subsequently measured using a bioluminescent substrate. Comparison of the detected ATP levels between noninduced cells and RNAi-induced cells revealed a major reduction in mt ATP by ~75% and ~94% at days 3 and 5 after RNAi induction, respectively (Fig. 4A). Additional controls were included to demonstrate that the production of ATP by oxidative phosphorylation was sensitive to malonate, an inhibitor of succinate dehydrogenase, and that all three ATP production pathways were sensitive to atractyloside, a specific inhibitor of the ADP/ATP translocator. Samples with no ADP added served as a control to detect ATP produced from any of the remaining endogenous ADP molecules (Fig. 4A). Our results indicate that TbAAC is the only ADP/ATP carrier responsible for ADP influx into the mitochondrion of PF *T. brucei*.

Under specific conditions, AAC can also work in reverse, thereby importing ATP into the mitochondria. Therefore, we examined this ATP influx activity using digitonin-extracted mt vesicles that had been incubated with ATP. Through TbAAC activity, ATP is imported into the mitochondria, where it is immediately hydrolyzed to ADP and inorganic phosphate by ubiquitous ATPase activities. The amount of inorganic phosphate that is created is then assessed spectrophotometrically to determine its concentration, which can then be used to calculate the ATPase activity in the sample due to the linear relationship between the two variables. Importantly, in TbAAC RNAi samples induced for 3 or 5 days, the total ATPase activity was decreased by ~20% or ~50%, respectively (Fig. 4B). Moreover, the total ATPase activity measured in cleared mt lysates (mt fractions with disrupted membranes) obtained from noninduced and RNAi-induced cells was unchanged (Fig. 4C). This result confirms that the decreased ATPase activity in the intact mt vesicles is not due to the general impairment of ATP hydrolytic protein complexes but rather is caused by the insufficient import of ATP into the mitochondria due to TbAAC ablation. However, it should be noted that the 50% reduction in ATP influx is not as high as one would expect, suggesting the presence of another carrier responsible for ATP influx into the mitochondria, possibly the ATP/P_i carrier.

TbAAC is crucial for the export of mt ATP into the cytosol. One of the most significant evolutionary events that allowed an engulfed alphaproteobacterium to become the organellar powerhouse of a eukaryotic cell depended on its ability to export ATP to the rest of the cell. Therefore, to determine if TbAAC is the principal exporter of ATP, we generated a TbAAC RNAi cell line that constitutively expresses firefly luciferase and allows us to measure cytosolic ATP levels *in vivo*. The amount of luciferase expression and its cytosolic localization in the LUC-TbAAC RNAi cell line was verified by Western blotting of digitonin-treated fractions (Fig. 5A). A commercial anti-luciferase antibody and antibodies recognizing the cytosolic enolase and mt Hsp70 protein were used to immunodecorate cytosolic and mt fractions, respectively. Once these LUC-TbAAC RNAi cells, either noninduced or induced for 3 days, were exposed to luciferin, the *in vivo* cytosolic ATP levels were measured by a luminometer. RNAi-mediated depletion of TbAAC severely decreased the level of cytosolic ATP compared to that in noninduced cells (Fig. 5B). Since the cytosolic ATP is significantly reduced (by 67%) after just 3 days of RNAi induction, when the growth phenotype is not yet fully manifested, we propose that the drop in the cytosolic ATP level is the primary reason for the impending growth retardation.

An imbalance in the mt ADP/ATP pool leads to an increased $\Delta\psi m$, an accumulation of ROS, and decreased respiration. The lack of ATP efflux activity from the organelle to the cytosol causes an aberrant mt ADP/ATP ratio, resulting from the limited availability of ADP and the accumulation of ATP in the mt matrix. This nucleotide imbalance likely impedes F_oF_1-ATP synthase activity, causing an mt inner membrane hyperpolarization that in turn alters other mt processes, such as respiration and ROS production. Therefore, these conventional organellar functions were examined as TbAAC was depleted. As predicted, the $\Delta\psi m$ was increased (up to 37% at day 5) in the RNAi-induced cells compared to noninduced controls (Fig. 6A; Table 1). Our previous *in vitro* assays demonstrated that the loss of TbAAC does not interfere with the ability of respiratory complexes III and IV to transmit electrons and presumably pump protons when they are provided the appropriate substrate. Therefore, this observed phenotype is likely due to the accumulation of protons in the intermembrane space, as the electrochemical potential of the proton motive force is never harnessed by the stagnant F_oF_1-ATP synthase that is lacking its ADP substrate.

In time, the increased $\Delta\psi m$ becomes so significant that respiration-coupled electron flow and proton pumping of complex III and IV become stalled. Consequently, we observed that the amount of ROS is dramatically elevated (210%) by day 5 of Tet-induced RNAi compared to noninduced samples (Fig. 6B; Table 1). This high level of oxidative stress likely contributes to the severe growth phenotype detected upon the knockdown of TbAAC. Furthermore, we determined that the total oxygen consumption is significantly decreased after 5 days of TbAAC depletion (Fig. 6C), most likely due to the hyperpolarization caused by the hindered

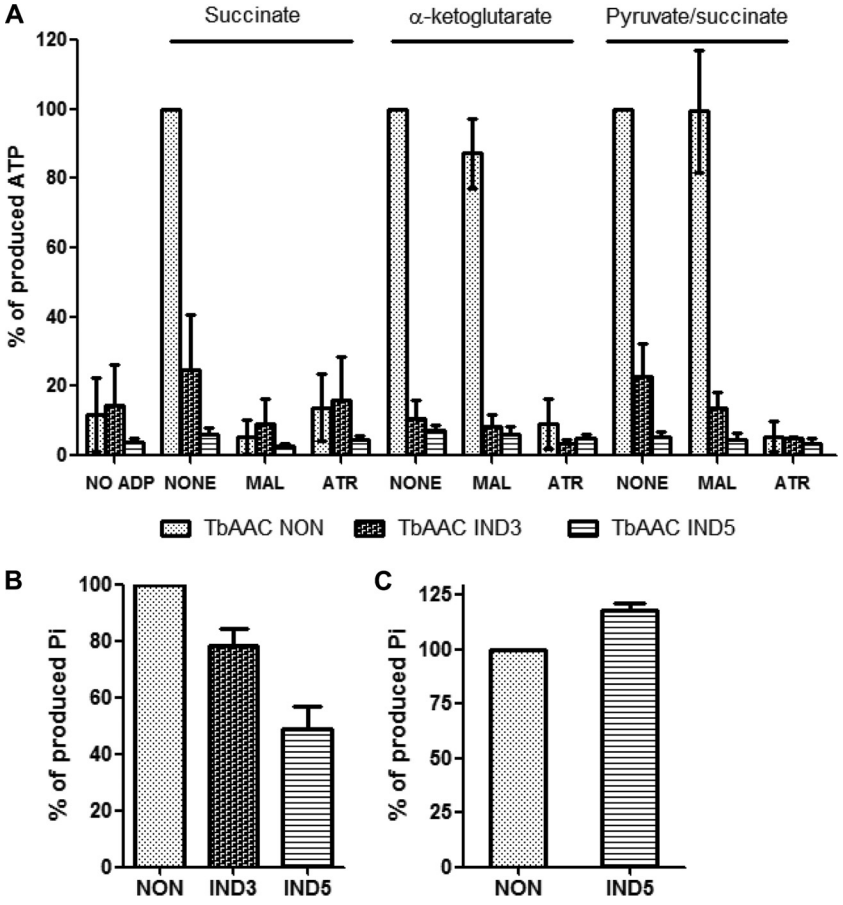

FIG 4 Both ADP and ATP influx into the mitochondrion are affected in cells silenced for TbAAC expression. (A) To determine levels of ADP influx into the mitochondrion, the *in vitro* production of ATP was measured in digitonin-extracted mitochondria from noninduced (NON) cells or cells with activated TbAAC RNAi for 3 (IND3) or 5 days (IND5). The phosphorylation pathways were triggered by the addition of ADP and one of the following substrates: succinate, α-ketoglutarate, and pyruvate/succinate. Malonate (MAL), a specific inhibitor of succinate dehydrogenase, was used to inhibit ATP production by oxidative phosphorylation, and atractyloside (ATR) was used to inhibit import of ADP into mitochondria. The level of ATP production in mitochondria isolated from noninduced RNAi cells stimulated with substrate, but in the absence of any specific inhibitors, was established as the reference and set to 100%. All other values for the same substrate are calculated arithmetic means expressed as percentages of this reference sample. The "No ADP" value serves as a control for the background production of ATP from endogenous mt ADP. The data are averages from at least three independent experiments and standard deviations. (B) To ascertain the extent of ATP import into active mitochondria, ATPase hydrolytic activities were measured in either noninduced (NON) TbAAC RNAi cells or cells induced with Tet for 3 (IND3) and 5 days (IND5). Crude mt vesicles were obtained by digitonin extraction. The ATPase activity was triggered by ATP addition (5 mM) and assayed by measuring the release of free phosphate. The total amount of free phosphate created from all ATPase enzymes present in the noninduced sample was set at 100%. The displayed results represent the average activities obtained from extracts prepared from four independent RNAi inductions. (C) Total ATPase activity measured in mitochondrial lysates from noninduced and RNAi cells induced for 5 days indicate that mt ATPases are still active when substrate is available. The total amount of free phosphate created from all ATPase enzymes present in the noninduced sample was set at 100%. The results are the average activities obtained from extracts prepared from four independent RNAi inductions.

activity of F_oF_1-ATP synthase. Importantly, there are two terminal oxidases (complex IV and trypanosome alternative oxidase [TAO]) in *T. brucei*, both of which can catalyze the final reduction of an oxygen molecule and thus contribute to the total oxygen consumption. While it is still unknown how electron flow is regulated between these two pathways, utilizing TAO allows the electrons to bypass respiratory complexes III and IV, which should help alleviate the damaging effects of ROS generated from an elevated $\Delta\psi m$. Nevertheless, we observed that complex IV contributed a majority of the respiration even in the presence of the excessive ROS created by day 5 in these TbAAC RNAi-induced cells (Fig. 6D). Strikingly, even the relative contribution of these two terminal oxidases to the overall cellular respiration was not significantly modified over time, suggesting that the activity of complex IV is not specifically inhibited by a high ADP/ATP ratio, as observed in mammalian mitochondria (51, 52).

Silencing of TbAAC leads to defects in cell division. In humans, the lack of AAC activity triggers mt DNA rearrangements and deletions followed by a complete loss of mt DNA (53, 54). To ascertain if a loss of mt DNA also occurs in *T. brucei* with downregulated TbAAC, the nuclear and mt DNA (termed kinetoplast DNA in these protists) were stained with DAPI and visualized by fluorescence microscopy (Fig. 7A). Trypanosomes in G_1 and S F7
phase possess one nucleus and one kinetoplast (1N1K), while in the G_2/M transition phase, these flagellates have one nucleus and two kinetoplasts (1N2K), as the mitochondrion division precedes mitosis. Finally, before undergoing cytokinesis, these cells have two nuclei and two kinetoplasts (2N2K) (Fig. 7A, top). In the

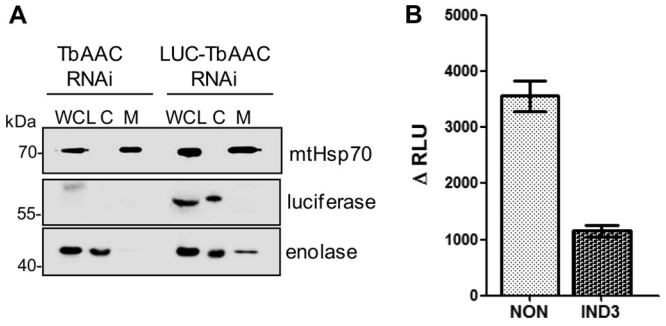

FIG 5 Cytosolic ATP levels are significantly decreased in TbAAC RNAi-induced cells. (A) The subcellular localization of luciferase was determined within TbAAC RNAi cells expressing luciferase (LUC-TbAAC RNAi). Parental TbAAC RNAi cells were used as a negative control. *T. brucei* cells (5×10^8) were harvested by centrifugation (WCL) and further separated into cytosolic (C) and mitochondrial (M) subcellular fractions upon digitonin extraction. Purified fractions were analyzed by Western blotting with anti-luciferase, anti-mt Hsp70 (mitochondria), and anti-enolase (cytosol) antibodies. The relevant sizes of the protein markers are on the left. (B) Total cytosolic ATP content was measured by a luminometer upon luciferin addition to living cells, either noninduced (NON) LUC-TbAAC RNAi cells or cells induced for 3 days (IND3). Values are in relative light units (RLU) and are averages from three independent RNAi inductions.

TABLE 1 $\Delta\psi m$ and ROS measurements[a]

Day	Fluorescence (%) of:	
	TMRE	DCFH-DA
3	119 ± 6	88 ± 25
5	137 ± 4	211 ± 20
7	125 ± 3	202 ± 21

[a] $\Delta\psi m$ and ROS were measured 3, 5, and 7 days after RNAi induction, using FACS analyses of the appropriate stain as described in Material and Methods. Data were obtained from at least three independent RNAi inductions. Fluorescence intensity in the RNAi-induced cells is expressed as a percentage of that in noninduced cells. Values are means and standard deviations.

noninduced control, 76% of the cells were found to have a single nucleus of normal size and a single kinetoplast (1N1K), while the rest (24%) were either 1N2K or 2N2K (Fig. 7B), which is representative of a healthy population of these parasites grown in culture. Importantly, even after 5 days of TbAAC RNAi induction, we did not observe a loss of mt DNA, in contrast to reports concerning mammals (55), but rather, we detected a substantial accumulation of cells with an aberrant number of nuclei and kinetoplasts. Examples of these abnormalities include anuclear cells (1K), as well as cells with two nuclei and one kinetoplast (2N1K) and larger monster cells with multiple nuclei and kinetoplasts (xNxK) (Fig. 7A, bottom). These results, quantified in Fig. 7B, suggest a failure

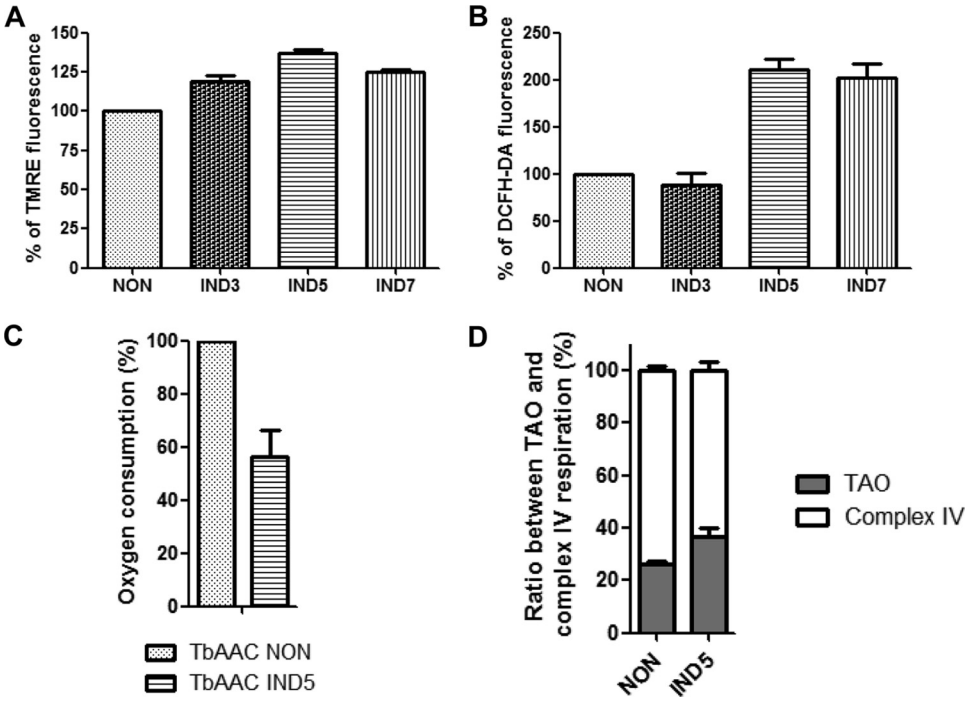

FIG 6 TbAAC silencing increases the $\Delta\psi m$, resulting in decreased oxygen consumption and elevated ROS production. (A) After staining with 60 nM TMRE, the $\Delta\psi m$ was measured by flow cytometry in both noninduced cells (NON) and TbAAC RNAi cells induced for 3 (IND3), 5 (IND5), and 7 (IND7) days. The median fluorescent intensity values are presented as percentages of the value for the noninduced sample, which was set to 100%. Data were obtained from at least three independent RNAi experiments, and the standard deviations are included. (B) The ROS detection reagent DCFH-DA was quantified by fluorescence-activated cell sorting (FACS) analysis in noninduced (NON) cells and TbAAC RNAi cells induced for 3 (IND3), 5 (IND5), and 7 (IND7) days. Increased fluorescence intensity corresponds to an accumulated ROS formation that was observed in three independent assays. (C) The oxygen consumption of noninduced (NON) and RNAi-induced (IND5) cells incubated in SDM-79 medium at 27°C was monitored with a Clark-type oxygen electrode. The total oxygen consumption in noninduced cells was set to 100%. Values are arithmetic means and standard deviations from three experiments. (D) The ratio of complex IV- and TAO-mediated respiration was measured in noninduced (NON) and TbAAC RNAi cells induced for 5 days (IND5). The total oxygen consumption in both cell lines was set to 100%. After the addition of SHAM (0.03 mM), a potent TAO inhibitor, the remaining oxygen consumption represented respiration occurring via complex IV. Values are means and standard deviations from six independent experiments.

AQ: Q

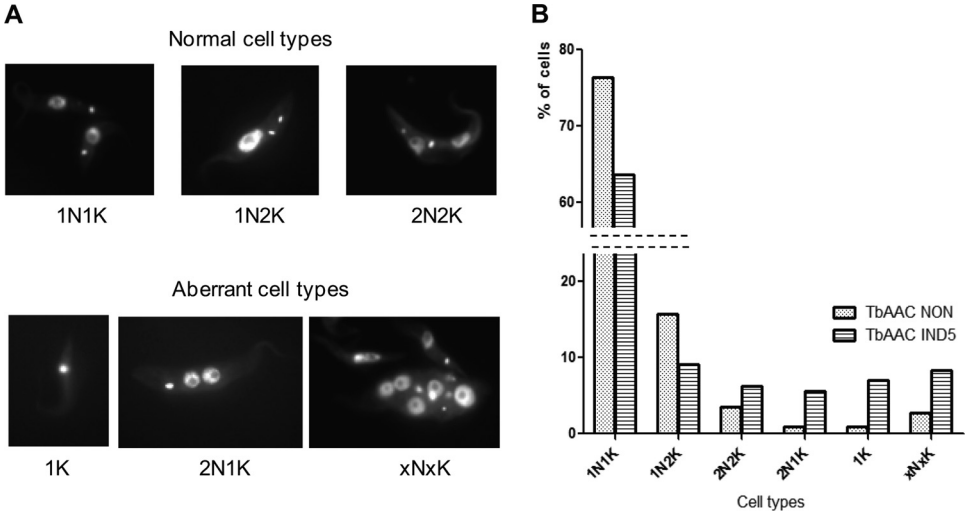

FIG 7 TbAAC depletion leads to defects in cell division. (A) DAPI staining was used to visualize various nucleus/kinetoplast (NK) phenotypes in noninduced TbAAC RNAi cells and cells induced with Tet for 5 days. (Top) Normal cell types either in G_1/S (1N1K) and G_2/M (1N2K) phases or undergoing cytokinesis (2N2K). (Bottom) Representative abnormal cell types (1K, 2N1K, and xNxK). N, nucleus; K, kinetoplast. (B) Quantification of the microscopy images based on the number of nuclei and kinetoplasts in more than 200 cells per time point. NON, noninduced cells; IND5, RNAi cells induced for 5 days.

in the overall cell division machinery, an effect likely to be caused by the shortage of cytosolic ATP.

DISCUSSION

In this study, we analyzed the functional and structural interactome of the mt ADP/ATP carrier in the insect stage of *T. brucei*, a highly diverged eukaryote. During this life stage, the parasite possesses an aerobically active mitochondrion that contains a fully developed respiratory chain coupled to ATP production by the F_oF_1-ATP synthase (17). Thus, in agreement with this mt function, silencing of TbAAC caused a decreased level of cytosolic ATP, a higher $\Delta\psi m$, an elevated amount of ROS, and a reduced consumption of oxygen. We further established that TbAAC functions as a physically separate entity and its downregulation does not impair the activity or arrangement of the OXPHOS components. Our results suggest that the energy demands during this stage of the parasite do not necessitate the incorporation of AAC into the respiratory supercomplexes.

The majority of the literature describing respiratory supercomplexes focuses on two main assemblies, either the dimeric F_oF_1-ATP synthase or the union of proton translocating complexes I, III, and IV. The latter complexes are usually found to assemble into I+III_2, III_2+IV_{1-2}, and I+III_2+IV_{2-4} supramolecular organizations, and their formation is well documented for only a few representatives of the supergroups Opisthokonta (*Saccharomyces cerevisiae*, *Yarrowia lipolytica*, *Bos taurus*, and *Homo sapiens*) and Archaeplastida (*Solanum tuberosum* and *Spinacia oleracea*) (56–59). It is believed that this physical association of the electron relay components creates patches within the mt inner membrane where the appropriate substrates can be concentrated, making the OXPHOS pathway more efficient to meet higher energy demands and decrease the potential for ROS formation. However, recent work with bovine mitochondria elegantly suggests that there is just one common pool of ubiquinone/ubiquinol and cytochrome *c*, which is free to interact with any OXPHOS components found in the protein-dense mt inner membrane (60). Whereas the interactions between respiratory supercomplexes appear to be quite delicate, the detection of the dimeric F_oF_1-ATP synthase has been more pervasive throughout the eukaryotic supergroups studied so far, including the protists of the supergroups Excavata and Alveolata (*T. brucei*, *Euglena gracilis*, *Plasmodium falciparum*, and *Tetrahymena thermophila*) (13, 61–64). This dimerization is proposed to be crucial for crista formation within the mt inner membrane (65), and the commonality of this structural organization in a wide variety of eukaryotes suggests that it was an early attempt to create microenvironments for components of the OXPHOS pathway.

To a lesser extent, the AAC has also been identified in special arrangements with some of these respiratory supercomplexes. In yeast, a large majority of the main ADP/ATP carrier, AAC2, physically interacts with a supercomplex comprised of III+IV and the TIM23 translocase, although this interaction is highly sensitive to the detergent type and its concentration (9). The mt ADP_{in}/ATP_{out} exchange under aerobic conditions is energetically costly because the efflux of ATP results in the expulsion of a net negative charge that partially collapses the $\Delta\psi m$. Thus, positioning AAC in a microenvironment packed with supercomplexes that contribute to a heightened local $\Delta\psi m$ may minimize this energetic cost, thus establishing a site that is conducive to maximum AAC transport activity. Furthermore, the OXPHOS pathway, specifically complex IV activity, is significantly downregulated in the absence of AAC2 (48), providing additional evidence for the energetic cost benefits of this supramolecular collaboration in yeast.

In *T. brucei* mitochondria, the migration of TbAAC also overlapped complex IV under low-detergent conditions in 2-D PAGE. However, this interaction was never detected in copurification assays that utilized lysis conditions nearly identical to those in the 2-D analysis. Furthermore, upon efficient TbAAC knockdown, we did not observe a decrease in the activity of complex IV, as seen in yeast (9). In fact, we consistently saw a slight increase in cytochrome *c* oxidase activity, as measured by in-gel staining or spectrophotometry assays, possibly due to a physiological response to an altered ADP/ATP ratio in the matrix. Importantly, the assem-

bly and integrity of the OXPHOS complexes and the steady-state abundance of their constituent subunits remained unchanged. These results significantly contrast those of studies performed in yeast, where, in the absence of AAC, the steady state of selected subunits of respiratory complex IV was diminished, and the assembly of the respiratory supercomplex (III_2+IV_2) was disrupted (9).

The association of AAC with the F_oF_1-ATP synthase and P_iC has been observed in highly enriched crista-like vesicles purified from rats (11, 12). In addition, it has been demonstrated that AAC and F_oF_1-ATP synthase in yeast cofractionate in CN or BN PAGE, implying that they also congregate into an ATP synthasome (49). Furthermore, cosedimentation and copurification studies of the F_oF_1-ATP synthase subunit β and AAC discerned a similar situation in *Leishmania mexicana*, a close relative of *T. brucei* (66). Contrary to these reports, our data do not support the existence of an ATP synthasome in *T. brucei*, as TbAAC did not copurify with tagged F_oF_1-ATP synthase subunit β or p18. Moreover, TbP_iC did not cosediment with the large molecular signals detected for TbAAC and subunit β in hrCN PAGE or with subunit β in glycerol gradients. While the authors are quick to acknowledge that the absence of an interaction does not prove that it does not exist, we were careful to perform reciprocal copurification assays using a less harsh detergent and the low salt concentrations used in the *Leishmania* study.

Perhaps this intriguing difference between these two closely related parasites is the result of the environments they encounter during their distinctive life cycles. While *Leishmania* possesses a fully developed mitochondrion throughout its life cycle due to the persistent requirement for the OXPHOS pathway (67), the morphology of the *T. brucei* mitochondrion is more pleomorphic, as the parasite transitions between the tsetse fly vector and the mammalian host's bloodstream. It is during the infectious stage that the mitochondrion becomes greatly reduced, containing many fewer cristae, which is indicative of its independence of the OXPHOS pathway for energy production in this high-glucose environment. Therefore, a closer inspection of the energetic demands and mechanisms to cope with ROS in these two protists might help to uncover the evolutionary forces that necessitate the assembly of this more efficient respiratory complex. In fact, purification of the *Leishmania* F_oF_1-ATP synthase might identify components absent from the *T. brucei* complex that are important for the interaction with P_iC and AAC.

The *T. brucei* genome encodes a singly functional ADP/ATP carrier, whose function has been confirmed by a complementation assay of an AAC2-deficient yeast strain. Furthermore, TbAAC biochemical properties and ADP/ATP exchange kinetics are similar to those of the yeast AAC2 carrier (26). Similar to the study done by Pena-Diaz and coworkers (26), our *in vitro* data assaying ADP influx into the mitochondrion for oxidative and substrate phosphorylation support these data, as ADP import into the organelle ceases upon an efficient TbAAC knockdown. Interestingly, when we measured the reverse function of this transporter, mainly the ATP import into the mitochondrion, we observed only a 51% decrease in the ATP-induced ATPase activity, suggesting the existence of another mt import route for ATP. An obvious candidate for such an activity would be a homolog of the ATP-Mg/P_i transporter, a protein that is responsible for the electroneutral exchange between ATP-Mg^{2-} and HPO_4^{2-}, which can supplement the mt ATP pool in cells using the hydrolytic activity of F_oF_1-ATPase to maintain the $\Delta\psi m$ (68). However, a putative *T. brucei* homolog of the ATP-Mg/P_i transporter (Tb927.4.1660, MCP6) was shown to be inactive for ATP and ADP transport (25, 69). Thus, besides TbAAC, any additional carrier(s) responsible for ATP influx into the mitochondria of this excavate protist remains to be elucidated.

The genome of *S. cerevisiae* contains three AAC genes: AAC1, AAC2, and AAC3 (70, 71). However, only the disruption of AAC2 triggers a growth phenotype when the yeast is grown on nonfermentable carbon sources (72). Notably, in the absence of AAC2, the downregulation of the ADP/ATP exchange across the mt inner membrane is followed by a reduction in oxygen consumption and a decrease in complex IV activity (9). A similar phenomenon has been described for human mitochondria, which also contain three isoforms of the adenine nucleotide translocase (ANT) (73). While the loss of the main ANT1 isoform is not lethal, it does induce mt myopathy, as the lack of ADP/ATP exchange activity depletes matrix ADP, which causes F_oF_1-ATP synthase stagnation (74, 75). Consequently, the flow of protons back to the matrix is blocked and the $\Delta\psi m$ increases until it reaches a level that prohibits oxidative phosphorylation, resulting in increased ROS production and mt DNA damage (76). Furthermore, mutations in the human ANT1 gene cause autosomal dominant progressive external ophthalmoplegia (adPEO), an mt disorder characterized by reduced respiration, lowered mt cytochrome content, and mt DNA deletions (54, 77). Moreover, this loss of mt DNA can further exacerbate the adPEO disorder by compromising the synthesis of specific respiratory subunits (75).

Trypanosomes depleted of TbAAC1 also displayed an elevated $\Delta\psi m$, decreased oxygen consumption, and heightened levels of ROS. However, in contrast to the yeast and human data, we did not observe a reduction in the activity or integrity of cytochrome-containing complexes III and IV. Therefore, the diminished respiration measured in TbAAC RNAi cells is not caused by the destabilization of the OXPHOS complexes, suggesting that even though high levels of ROS are detected, they do not seem to have deleterious effects on the mt DNA. To verify this outcome, the DNA content was examined by fluorescence microscopy in TbAAC-depleted cells. Although mt DNA rearrangements, deletions, and total loss were identified in humans with adPEO ANT1 mutations (55), we did not observe a complete loss of mt DNA. Instead, we detected decreased populations of normal cells in the G_1 or S phase with a concurrent accumulation of cells with an aberrant number of nuclei and/or kinetoplasts or parasites apparently arrested in a state of incomplete cytokinesis. In their totality, these results indicate that the loss of TbAAC in *T. brucei* does not result in the targeted loss of mt genes but rather leads to general defects in cell cycle control or division due to an overall cellular depletion of ATP.

While identifying the often delicate interaction of AAC with components of the OXPHOS pathway is challenging, the totality of this work suggests that TbAAC does not interact with F_oF_1-ATP synthase in *T. brucei* as it does in its close relative, *L. mexicana*. It would be interesting to investigate if the association of TbAAC, TbP_iC, and F_oF_1-ATPase (F_oF_1-ATP hydrolasome) exists in the infectious bloodstream stage of *T. brucei*, where the $\Delta\psi m$ depends on ATP hydrolysis by the F_oF_1-ATPase located in an environment lacking significant cristae and the microenvironments they create.

ACKNOWLEDGMENTS

We thank Ken Stuart (Seattle Biomed) for kindly providing anti-mt Hsp70 antibody. We express our gratitude to Zdeněk Paris and Zdeněk Verner for their contribution at the initial stage of this study.

This work was funded by Ministry of Education ERC CZ grant LL1205, Czech Grant Agency grant P302/12/2513, EMBO Installation grant 1965 to A.Z., and the Praemium Academiae award to J.L. and by the Slovak Research and Development Agency under contract APVV-0286-12 and the Scientific Grant Agency of the Slovak Ministry of Education and the Academy of Sciences 1/0664/13 to A.H. We acknowledge the use of research infrastructure that has received funding from the European Union Seventh Framework Programme (FP7/2007-2013) under grant agreement no. 316304.

REFERENCES

1. **Arco AD, Satrustegui J.** 2005. New mitochondrial carriers: an overview. Cell Mol Life Sci **62:**2204–2227. http://dx.doi.org/10.1007/s00018-005-5197-x.
2. **Klingenberg M.** 2008. The ADP and ATP transport in mitochondria and its carrier. Biochim Biophys Acta **1778:**1978–2021. http://dx.doi.org/10.1016/j.bbamem.2008.04.011.
3. **Dudkina NV, Kouril R, Peters K, Braun HP, Boekema EJ.** 2010. Structure and function of mitochondrial supercomplexes. Biochim Biophys Acta **1797:**664–670. http://dx.doi.org/10.1016/j.bbabio.2009.12.013.
4. **Dudkina NV, Heinemeyer J, Sunderhaus S, Boekema EJ, Braun HP.** 2006. Respiratory chain supercomplexes in the plant mitochondrial membrane. Trends Plant Sci **11:**232–240. http://dx.doi.org/10.1016/j.tplants.2006.03.007.
5. **Minauro-Sanmiguel F, Wilkens S, Garcia JJ.** 2005. Structure of dimeric mitochondrial ATP synthase: novel F0 bridging features and the structural basis of mitochondrial cristae biogenesis. Proc Natl Acad Sci U S A **102:**12356–12358. http://dx.doi.org/10.1073/pnas.0503893102.
6. **Davies KM, Anselmi C, Wittig I, Faraldo-Gomez JD, Kuhlbrandt W.** 2012. Structure of the yeast F1Fo-ATP synthase dimer and its role in shaping the mitochondrial cristae. Proc Natl Acad Sci U S A **109:**13602–13607. http://dx.doi.org/10.1073/pnas.1204593109.
7. **Bamber L, Harding M, Monne M, Slotboom DJ, Kunji ER.** 2007. The yeast mitochondrial ADP/ATP carrier functions as a monomer in mitochondrial membranes. Proc Natl Acad Sci U S A **104:**10830–10834. http://dx.doi.org/10.1073/pnas.0703969104.
8. **Nury H, Dahout-Gonzalez C, Trezeguet V, Lauquin G, Brandolin G, Pebay-Peyroula E.** 2005. Structural basis for lipid-mediated interactions between mitochondrial ADP/ATP carrier monomers. FEBS Lett **579:**6031–6036. http://dx.doi.org/10.1016/j.febslet.2005.09.061.
9. **Dienhart MK, Stuart RA.** 2008. The yeast Aac2 protein exists in physical association with the cytochrome bc1-COX supercomplex and the TIM23 machinery. Mol Biol Cell **19:**3934–3943. http://dx.doi.org/10.1091/mbc.E08-04-0402.
10. **Mehnert CS, Rampelt H, Gebert M, Oeljeklaus S, Schrempp SG, Kochbeck L, Guiard B, Warscheid B, van der Laan M.** 2014. The mitochondrial ADP/ATP carrier associates with the inner membrane presequence translocase in a stoichiometric manner. J Biol Chem **289:**27352–27362. http://dx.doi.org/10.1074/jbc.M114.556498.
11. **Chen C, Ko Y, Delannoy M, Ludtke SJ, Chiu W, Pedersen PL.** 2004. Mitochondrial ATP synthasome: three-dimensional structure by electron microscopy of the ATP synthase in complex formation with carriers for Pi and ADP/ATP. J Biol Chem **279:**31761–31768. http://dx.doi.org/10.1074/jbc.M401353200.
12. **Ko YH, Delannoy M, Hullihen J, Chiu W, Pedersen PL.** 2003. Mitochondrial ATP synthasome. Cristae-enriched membranes and a multiwell detergent screening assay yield dispersed single complexes containing the ATP synthase and carriers for Pi and ADP/ATP. J Biol Chem **278:**12305–12309. http://dx.doi.org/10.1074/jbc.C200703200.
13. **Acestor N, Zíková A, Dalley RA, Anupama A, Panigrahi AK, Stuart KD.** 2011. Trypanosoma brucei mitochondrial respiratome: composition and organization in procyclic form. Mol Cell Proteomics **10:**M110.006908. http://dx.doi.org/10.1074/mcp.M110.006908.
14. **Simarro PP, Jannin J, Cattand P.** 2008. Eliminating human African trypanosomiasis: where do we stand and what comes next? PLoS Med **5:**e55. http://dx.doi.org/10.1371/journal.pmed.0050055.
15. **Fevre EM, Wissmann BV, Welburn SC, Lutumba P.** 2008. The burden of human African trypanosomiasis. PLoS Negl Trop Dis **2:**e333. http://dx.doi.org/10.1371/journal.pntd.0000333.
16. **Tielens AG, van Hellemond JJ.** 2009. Surprising variety in energy metabolism within Trypanosomatidae. Trends Parasitol **25:**482–490. http://dx.doi.org/10.1016/j.pt.2009.07.007.
17. **Besteiro S, Barrett MP, Riviere L, Bringaud F.** 2005. Energy generation in insect stages of Trypanosoma brucei: metabolism in flux. Trends Parasitol **21:**185–191. http://dx.doi.org/10.1016/j.pt.2005.02.008.
18. **Zíková A, Schnaufer A, Dalley RA, Panigrahi AK, Stuart KD.** 2009. The F(0)F(1)-ATP synthase complex contains novel subunits and is essential for procyclic Trypanosoma brucei. PLoS Pathog **5:**e1000436. http://dx.doi.org/10.1371/journal.ppat.1000436.
19. **Bochud-Allemann N, Schneider A.** 2002. Mitochondrial substrate level phosphorylation is essential for growth of procyclic Trypanosoma brucei. J Biol Chem **277:**32849–32854. http://dx.doi.org/10.1074/jbc.M205776200.
20. **Hannaert V, Bringaud F, Opperdoes FR, Michels PA.** 2003. Evolution of energy metabolism and its compartmentation in Kinetoplastida. Kinetoplastid Biol Dis **2:**11. http://dx.doi.org/10.1186/1475-9292-2-11.
21. **Fang J, Beattie DS.** 2003. Identification of a gene encoding a 54 kDa alternative NADH dehydrogenase in Trypanosoma brucei. Mol Biochem Parasitol **127:**73–77. http://dx.doi.org/10.1016/S0166-6851(02)00305-5.
22. **Chaudhuri M, Ott RD, Hill GC.** 2006. Trypanosome alternative oxidase: from molecule to function. Trends Parasitol **22:**484–491. http://dx.doi.org/10.1016/j.pt.2006.08.007.
23. **Nolan DP, Voorheis HP.** 1992. The mitochondrion in bloodstream forms of Trypanosoma brucei is energized by the electrogenic pumping of protons catalysed by the F1F0-ATPase. Eur J Biochem **209:**207–216. http://dx.doi.org/10.1111/j.1432-1033.1992.tb17278.x.
24. **Schnaufer A, Clark-Walker GD, Steinberg AG, Stuart K.** 2005. The F1-ATP synthase complex in bloodstream stage trypanosomes has an unusual and essential function. EMBO J **24:**4029–4040. http://dx.doi.org/10.1038/sj.emboj.7600862.
25. **Colasante C, Pena Diaz P, Clayton C, Voncken F.** 2009. Mitochondrial carrier family inventory of Trypanosoma brucei brucei: identification, expression and subcellular localisation. Mol Biochem Parasitol **167:**104–117. http://dx.doi.org/10.1016/j.molbiopara.2009.05.004.
26. **Pena-Diaz P, Pelosi L, Ebikeme C, Colasante C, Gao F, Bringaud F, Voncken F.** 2012. Functional characterization of TbMCP5, a conserved and essential ADP/ATP carrier present in the mitochondrion of the human pathogen Trypanosoma brucei. J Biol Chem **287:**41861–41874. http://dx.doi.org/10.1074/jbc.M112.404699.
27. **Verner Z, Basu S, Benz C, Dixit S, Dobáková E, Faktorová D, Hashimi H, Horáková E, Huang Z, Paris Z, Peña-Diaz P, Ridlon L, Týč J, Wildridge D, Zíková A, Lukeš J.** The malleable mitochondrion of Trypanosoma brucei. Int Rev Cell Mol Biol, in press. AQ: N
28. **Wickstead B, Ersfeld K, Gull K.** 2002. Targeting of a tetracycline-inducible expression system to the transcriptionally silent minichromosomes of Trypanosoma brucei. Mol Biochem Parasitol **125:**211–216. http://dx.doi.org/10.1016/S0166-6851(02)00238-4.
29. **Flaspohler JA, Jensen BC, Saveria T, Kifer CT, Parsons M.** 2010. A novel protein kinase localized to lipid droplets is required for droplet biogenesis in trypanosomes. Eukaryot Cell **9:**1702–1710. http://dx.doi.org/10.1128/EC.00106-10.
30. **Wirtz E, Leal S, Ochatt C, Cross GA.** 1999. A tightly regulated inducible expression system for conditional gene knock-outs and dominant-negative genetics in Trypanosoma brucei. Mol Biochem Parasitol **99:**89–101. http://dx.doi.org/10.1016/S0166-6851(99)00002-X.
31. **Surve S, Heestand M, Panicucci B, Schnaufer A, Parsons M.** 2012. Enigmatic presence of mitochondrial complex I in Trypanosoma brucei bloodstream forms. Eukaryot Cell **11:**183–193. http://dx.doi.org/10.1128/EC.05282-11.
32. **Panigrahi AK, Ogata Y, Zíková A, Anupama A, Dalley RA, Acestor N, Myler PJ, Stuart KD.** 2009. A comprehensive analysis of Trypanosoma brucei mitochondrial proteome. Proteomics **9:**434–450. http://dx.doi.org/10.1002/pmic.200800477.
33. **Horváth A, Horáková E, Dunajcíková P, Verner Z, Pravdová E, Slapetová I, Cuninková L, Lukes J.** 2005. Downregulation of the nuclear-encoded subunits of the complexes III and IV disrupts their respective complexes but not complex I in procyclic Trypanosoma brucei. Mol Microbiol **58:**116–130. http://dx.doi.org/10.1111/j.1365-2958.2005.04813.x.
34. **Wittig I, Karas M, Schagger H.** 2007. High resolution clear native electrophoresis for in-gel functional assays and fluorescence studies of mem-

brane protein complexes. Mol Cell Proteomics **6:**1215–1225. http://dx.doi.org/10.1074/mcp.M700076-MCP200.

35. **Maslov DA, Zíková A, Kyselova I, Lukeš J.** 2002. A putative novel nuclear-encoded subunit of the cytochrome c oxidase complex in trypanosomatids. Mol Biochem Parasitol **125:**113–125. http://dx.doi.org/10.1016/S0166-6851(02)00235-9.
36. **Hannaert V, Albert MA, Rigden DJ, da Silva Giotto MT, Thiemann O, Garratt RC, Van Roy J, Opperdoes FR, Michels PA.** 2003. Kinetic characterization, structure modelling studies and crystallization of Trypanosoma brucei enolase. Eur J Biochem **270:**3205–3213. http://dx.doi.org/10.1046/j.1432-1033.2003.03692.x.
37. **Panigrahi AK, Zíková A, Dalley RA, Acestor N, Ogata Y, Anupama A, Myler PJ, Stuart KD.** 2008. Mitochondrial complexes in Trypanosoma brucei: a novel complex and a unique oxidoreductase complex. Mol Cell Proteomics **7:**534–545. http://dx.doi.org/10.1074/mcp.M700430-MCP200.
38. **Priest JW, Hajduk SL.** 2003. Trypanosoma brucei cytochrome c1 is imported into mitochondria along an unusual pathway. J Biol Chem **278:**15084–15094. http://dx.doi.org/10.1074/jbc.M212956200.
39. **Šubrtová K, Panicucci B, Zíková A.** ATPaseTb2, a unique membrane-bound FoF1-ATPase component, is essential in bloodstream and dyskinetoplastic trypanosomes. PLoS Pathog, in press.

AQ: O

40. **Zíková A, Panigrahi AK, Uboldi AD, Dalley RA, Handman E, Stuart K.** 2008. Structural and functional association of Trypanosoma brucei MIX protein with cytochrome c oxidase complex. Eukaryot Cell **7:**1994–2003. http://dx.doi.org/10.1128/EC.00204-08.
41. **Gnipova A, Panicucci B, Paris Z, Verner Z, Horvath A, Lukeš J, Zíková A.** 2012. Disparate phenotypic effects from the knockdown of various Trypanosoma brucei cytochrome c oxidase subunits. Mol Biochem Parasitol **184:**90–98. http://dx.doi.org/10.1016/j.molbiopara.2012.04.013.
42. **Allemann N, Schneider A.** 2000. ATP production in isolated mitochondria of procyclic Trypanosoma brucei. Mol Biochem Parasitol **111:**87–94. http://dx.doi.org/10.1016/S0166-6851(00)00303-0.
43. **Tan TH, Bochud-Allemann N, Horn EK, Schneider A.** 2002. Eukaryotic-type elongator tRNAMet of Trypanosoma brucei becomes formylated after import into mitochondria. Proc Natl Acad Sci U S A **99:**1152–1157. http://dx.doi.org/10.1073/pnas.022522299.
44. **Law RH, Manon S, Devenish RJ, Nagley P.** 1995. ATP synthase from Saccharomyces cerevisiae. Methods Enzymol **260:**133–163. http://dx.doi.org/10.1016/0076-6879(95)60135-X.
45. **de Wet JR, Wood KV, DeLuca M, Helinski DR, Subramani S.** 1987. Firefly luciferase gene: structure and expression in mammalian cells. Mol Cell Biol **7:**725–737.
46. **Maechler P, Wang H, Wollheim CB.** 1998. Continuous monitoring of ATP levels in living insulin secreting cells expressing cytosolic firefly luciferase. FEBS Lett **422:**328–332. http://dx.doi.org/10.1016/S0014-5793(97)01618-9.
47. **Saddar S, Dienhart MK, Stuart RA.** 2008. The F1F0-ATP synthase complex influences the assembly state of the cytochrome bc1-cytochrome oxidase supercomplex and its association with the TIM23 machinery. J Biol Chem **283:**6677–6686. http://dx.doi.org/10.1074/jbc.M708440200.
48. **Claypool SM, Oktay Y, Boontheung P, Loo JA, Koehler CM.** 2008. Cardiolipin defines the interactome of the major ADP/ATP carrier protein of the mitochondrial inner membrane. J Cell Biol **182:**937–950. http://dx.doi.org/10.1083/jcb.200801152.
49. **Wittig I, Schagger H.** 2008. Structural organization of mitochondrial ATP synthase. Biochim Biophys Acta **1777:**592–598. http://dx.doi.org/10.1016/j.bbabio.2008.04.027.
50. **Kawamata H, Starkov AA, Manfredi G, Chinopoulos C.** 2010. A kinetic assay of mitochondrial ADP-ATP exchange rate in permeabilized cells. Anal Biochem **407:**52–57. http://dx.doi.org/10.1016/j.ab.2010.07.031.
51. **Helling S, Vogt S, Rhiel A, Ramzan R, Wen L, Marcus K, Kadenbach B.** 2008. Phosphorylation and kinetics of mammalian cytochrome c oxidase. Mol Cell Proteomics **7:**1714–1724. http://dx.doi.org/10.1074/mcp.M800137-MCP200.
52. **Ramzan R, Staniek K, Kadenbach B, Vogt S.** 2010. Mitochondrial respiration and membrane potential are regulated by the allosteric ATP-inhibition of cytochrome c oxidase. Biochim Biophys Acta **1797:**1672–1680. http://dx.doi.org/10.1016/j.bbabio.2010.06.005.
53. **Kucejova B, Li L, Wang X, Giannattasio S, Chen XJ.** 2008. Pleiotropic effects of the yeast Sal1 and Aac2 carriers on mitochondrial function via an activity distinct from adenine nucleotide transport. Mol Genet Genomics **280:**25–39. http://dx.doi.org/10.1007/s00438-008-0342-5.
54. **Wang X, Salinas K, Zuo X, Kucejova B, Chen XJ.** 2008. Dominant membrane uncoupling by mutant adenine nucleotide translocase in mitochondrial diseases. Hum Mol Genet **17:**4036–4044. http://dx.doi.org/10.1093/hmg/ddn306.
55. **Kaukonen J, Juselius JK, Tiranti V, Kyttala A, Zeviani M, Comi GP, Keranen S, Peltonen L, Suomalainen A.** 2000. Role of adenine nucleotide translocator 1 in mtDNA maintenance. Science **289:**782–785. http://dx.doi.org/10.1126/science.289.5480.782.
56. **Schagger H, Pfeiffer K.** 2000. Supercomplexes in the respiratory chains of yeast and mammalian mitochondria. EMBO J **19:**1777–1783. http://dx.doi.org/10.1093/emboj/19.8.1777.
57. **Nubel E, Wittig I, Kerscher S, Brandt U, Schagger H.** 2009. Two-dimensional native electrophoretic analysis of respiratory supercomplexes from Yarrowia lipolytica. Proteomics **9:**2408–2418. http://dx.doi.org/10.1002/pmic.200800632.
58. **Bultema JB, Braun HP, Boekema EJ, Kouril R.** 2009. Megacomplex organization of the oxidative phosphorylation system by structural analysis of respiratory supercomplexes from potato. Biochim Biophys Acta **1787:**60–67. http://dx.doi.org/10.1016/j.bbabio.2008.10.010.
59. **Krause F, Reifschneider NH, Vocke D, Seelert H, Rexroth S, Dencher NA.** 2004. "Respirasome"-like supercomplexes in green leaf mitochondria of spinach. J Biol Chem **279:**48369–48375. http://dx.doi.org/10.1074/jbc.M406085200.
60. **Blaza JN, Serreli R, Jones AJ, Mohammed K, Hirst J.** 2014. Kinetic evidence against partitioning of the ubiquinone pool and the catalytic relevance of respiratory-chain supercomplexes. Proc Natl Acad Sci U S A **111:**15735–15740. http://dx.doi.org/10.1073/pnas.1413855111.
61. **Chaban Y, Boekema EJ, Dudkina NV.** 2014. Structures of mitochondrial oxidative phosphorylation supercomplexes and mechanisms for their stabilisation. Biochim Biophys Acta **1837:**418–426. http://dx.doi.org/10.1016/j.bbabio.2013.10.004.
62. **Balabaskaran Nina P, Dudkina NV, Kane LA, van Eyk JE, Boekema EJ, Mather MW, Vaidya AB.** 2010. Highly divergent mitochondrial ATP synthase complexes in Tetrahymena thermophila. PLoS Biol **8:**e1000418. http://dx.doi.org/10.1371/journal.pbio.1000418.
63. **Balabaskaran Nina P, Morrisey JM, Ganesan SM, Ke H, Pershing AM, Mather MW, Vaidya AB.** 2011. ATP synthase complex of Plasmodium falciparum: dimeric assembly in mitochondrial membranes and resistance to genetic disruption. J Biol Chem **286:**41312–41322. http://dx.doi.org/10.1074/jbc.M111.290973.
64. **Perez E, Lapaille M, Degand H, Cilibrasi L, Villavicencio-Queijeiro A, Morsomme P, Gonzalez-Halphen D, Field MC, Remacle C, Baurain D, Cardol P.** 2014. The mitochondrial respiratory chain of the secondary green alga Euglena gracilis shares many additional subunits with parasitic Trypanosomatidae. Mitochondrion **19:**338–349. http://dx.doi.org/10.1016/j.mito.2014.02.001.
65. **Paumard P, Vaillier J, Coulary B, Schaeffer J, Soubannier V, Mueller DM, Brethes D, di Rago JP, Velours J.** 2002. The ATP synthase is involved in generating mitochondrial cristae morphology. EMBO J **21:**221–230. http://dx.doi.org/10.1093/emboj/21.3.221.
66. **Detke S, Elsabrouty R.** 2008. Identification of a mitochondrial ATP synthase-adenine nucleotide translocator complex in Leishmania. Acta Trop **105:**16–20. http://dx.doi.org/10.1016/j.actatropica.2007.08.008.
67. **Opperdoes FR, Coombs GH.** 2007. Metabolism of Leishmania: proven and predicted. Trends Parasitol **23:**149–158. http://dx.doi.org/10.1016/j.pt.2007.02.004.
68. **Traba J, Froschauer EM, Wiesenberger G, Satrustegui J, Del Arco A.** 2008. Yeast mitochondria import ATP through the calcium-dependent ATP-Mg/Pi carrier Sal1p, and are ATP consumers during aerobic growth in glucose. Mol Microbiol **69:**570–585. http://dx.doi.org/10.1111/j.1365-2958.2008.06300.x.
69. **Colasante C, Alibu VP, Kirchberger S, Tjaden J, Clayton C, Voncken F.** 2006. Characterization and developmentally regulated localization of the mitochondrial carrier protein homologue MCP6 from Trypanosoma brucei. Eukaryot Cell **5:**1194–1205. http://dx.doi.org/10.1128/EC.00096-06.
70. **Lawson JE, Douglas MG.** 1988. Separate genes encode functionally equivalent ADP/ATP carrier proteins in Saccharomyces cerevisiae. Isolation and analysis of AAC2. J Biol Chem **263:**14812–14818.
71. **Kolarov J, Kolarova N, Nelson N.** 1990. A third ADP/ATP translocator gene in yeast. J Biol Chem **265:**12711–12716.
72. **Drgon T, Sabova L, Gavurnikova G, Kolarov J.** 1992. Yeast ADP/ATP carrier (AAC) proteins exhibit similar enzymatic properties but their deletion produces different phenotypes. FEBS Lett **304:**277–280. http://dx.doi.org/10.1016/0014-5793(92)80637-V.

73. **Stepien G, Torroni A, Chung AB, Hodge JA, Wallace DC.** 1992. Differential expression of adenine nucleotide translocator isoforms in mammalian tissues and during muscle cell differentiation. J Biol Chem **267:** 14592–14597.
74. **Echaniz-Laguna A, Chassagne M, Ceresuela J, Rouvet I, Padet S, Acquaviva C, Nataf S, Vinzio S, Bozon D, Mousson de Camaret B.** 2012. Complete loss of expression of the ANT1 gene causing cardiomyopathy and myopathy. J Med Genet **49:**146–150. http://dx.doi.org/10.1136/jmedgenet-2011-100504.
75. **Palmieri L, Alberio S, Pisano I, Lodi T, Meznaric-Petrusa M, Zidar J, Santoro A, Scarcia P, Fontanesi F, Lamantea E, Ferrero I, Zeviani M.** 2005. Complete loss-of-function of the heart/muscle-specific adenine nucleotide translocator is associated with mitochondrial myopathy and cardiomyopathy. Hum Mol Genet **14:**3079–3088. http://dx.doi.org/10.1093/hmg/ddi341.
76. **Esposito LA, Melov S, Panov A, Cottrell BA, Wallace DC.** 1999. Mitochondrial disease in mouse results in increased oxidative stress. Proc Natl Acad Sci U S A **96:**4820–4825. http://dx.doi.org/10.1073/pnas.96.9.4820.
77. **Fontanesi F, Palmieri L, Scarcia P, Lodi T, Donnini C, Limongelli A, Tiranti V, Zeviani M, Ferrero I, Viola AM.** 2004. Mutations in AAC2, equivalent to human adPEO-associated ANT1 mutations, lead to defective oxidative phosphorylation in Saccharomyces cerevisiae and affect mitochondrial DNA stability. Hum Mol Genet **13:**923–934. http://dx.doi.org/10.1093/hmg/ddh108.

JOBNAME: AUTHOR QUERIES PAGE: 1 SESS: 1 OUTPUT: Sat Jan 24 09:02:01 2015
/rich4/zek-euka/zek-euka/zek00315/zek4407d15z

AUTHOR QUERIES

AUTHOR PLEASE ANSWER ALL QUERIES 1

AQau—Please confirm the given-names and surnames are identified properly by the colors. ■= Given-Name, ■= Surname

AQaff—Please confirm the following full affiliations or correct here as necessary. This is what will appear in the online HTML version:

[a]Biology Center, Institute of Parasitology, Czech Academy of Sciences, České Budějovice, Czech Republic
[b]Department of Biochemistry, Faculty of Natural Sciences, Comenius University, Bratislava, Slovakia
[c]Faculty of Science, University of South Bohemia, České Budějovice, Czech Republic
[d]Canadian Institute for Advanced Research, Toronto, Ontario, Canada

AQaff—This affiliation line will appear in the PDF version of the article and matches that on page 1 of the proof; corrections to this affiliation line may be made here **or** on page 1 of the proof:

Biology Center, Institute of Parasitology, Czech Academy of Sciences, České Budějovice, Czech Republic[a]; Department of Biochemistry, Faculty of Natural Sciences, Comenius University, Bratislava, Slovakia[b]; Faculty of Science, University of South Bohemia, České Budějovice, Czech Republic[c]; Canadian Institute for Advanced Research, Toronto, Ontario, Canada[d]

AQA—If change of "it appears" to "this study showed" is not accurate, please specify what is in contrast to previous studies.

AQB—"origin" changed to "origination" for consistency with "event"; if this is not accurate, please provide another word that designates an event.

AQC—Please confirm that "tandem affinity purification (TAP)-tagged" is accurate (it implies that the subunits were tagged with purification), or clarify further what the subunits were tagged with.

AQD—Please confirm that "REV" (above, this paragraph) and "RV" are both correct, or mark the proof if a change is needed.

AQE—If "CLS" is an abbreviation, please write out what it stands for.

AQF—Please write out what "LUC" stands for.

AQG—If this sentence is not OK as edited, please make the necessary corrections on the proof.

AQH—If change of "was disappearing" to "disappeared" is not accurate, please clarify (e.g., do you mean "partially disappeared"?).

AQI—Per ASM policy, tables are generally required to have six or more data. The data from

AUTHOR QUERIES

AUTHOR PLEASE ANSWER ALL QUERIES

original Table 1 have therefore been incorporated into the text; please check the data and also the renumbering of original Table 2.

AQJ—Please confirm that the change of "b" to "β" is correct.

AQK—Please identify "the authors" (authors of ref 11 and 12, ref 49, or ref 66? All of these?).

AQL—If change of "sal1" to "salt" is not as meant, please correct the proof.

AQM—Genes encode but cannot be said to be encoded; "mt encoded genes" has been changed to "mt genes." If this is not correct/sufficient, please provide another wording in the proof.

AQN—If in-press reference is now published, please update (year, vol. no., page nos., and doi).

AQO—If in-press reference is now published, please update (year, vol. no., page nos., and doi).

AQP—Please confirm that the addition of "in thousands" is accurate.

AQQ—Please write out what SHAM stands for.